In Silico Study Of Organic Compounds From *Dipteryx Odorata* With SARS-COV-2 Targets By Molecular Docking And ADME-TOX Analysis

.

ABSTRACT

Introduction: The new coronavirus SARS-CoV-2 (severe acute respiratory syndrome coronavirus 2), identified in December 2019 as the cause of COVID-19, has triggered an outbreak of potentially fatal atypical pneumonia. The constant search for new molecules or strategies to combat this disease continues. Thus, the objective of this work was to evaluate, using in silico methods, the compounds present in *Dipteryx odorata* as inhibitors of crucial targets of SARS-COV-2.
Methodology: The methodology included the selection of plant compounds from the Pubchem database and obtaining the structures of SARS-COV-2 proteins (6vxx, 6lu7, 1R42) from the Protein Data Bank (PDB). The molecular docking analysis was performed using the Autodock Tools 1.5.6 and Autodock Vina programs, LigPlus to obtain amino acids, and Chimera v.13.1 to generate 3D images. The absorption, distribution, metabolism, excretion and toxicity (ADME-TOX) properties of the most promising compounds were evaluated with the pkCSM tool.
Results: In total, 672 molecular dockings were carried out, tested with 168 ligands, resulting in 17 compounds with binding energies lower than -7.9 kcal.mol^{-1}. A highlight was the exceptional interaction of the vouacapenic acid compound with the Spike protein, recording an energy of -9.9 kcal.mol^{-1}. The study revealed that compounds such as vouacapenic acid, taraxasterol and luteolin showed notable interactions with the Spike protein, in addition to positive results in the ADMET-TOX profile.
Conclusion: These findings indicate the potential of these compounds and point to the need for in vivo and in vitro studies to validate their antiviral efficacy as therapeutic agents against SARS-COV-2.

Keywords: Antiviral activity; COVID-19; medicinal chemistry; pharmacological properties; proteins.

1. INTRODUCTION

In December 2019, a novel coronavirus (CoV) was determined to be responsible for an outbreak of potentially fatal atypical pneumonia, defined as coronavirus disease-19 (COVID-19), in Wuhan, China. This disease is caused by the SARS-COV-2 virus, belonging to the severe acute respiratory syndrome coronavirus 2 (SARS-CoV-2) [1]. The SARS-COV-2 genome shares about 80% identity with SARS-CoV, responsible for the 2002 SARS pandemic, and about 96% similarity with the bat coronavirus BatCoV RaTG13 [2]. Since then, COVID-19 has spread globally, resulting in health and economic crises and infecting millions of people around the world.

We currently have vaccines developed as a preventive measure to achieve immunity to the virus, in addition to the repositioning of old medicines, representing a promising strategy in an attempt to combat the pandemic. Medicines such as remdesivir,

paxlovid, molnupiravir, baricitinib, among others, have been used to treat COVID- 19 [3]. However, the persistent need for innovative approaches and the identification of new molecules or strategies to combat the disease remains. Phytochemicals emerge as therapeutic and pharmacological agents of significant importance in the research and development of new drugs.

The species *Dipteryx odorata* Aubl Willd known as cumaru, is widely used in folk medicine. Belonging to the Fabaceae family, it receives different regional names, such as cumaru do Amazonas, cumbari sarrapia, cumaru purple, cumaru-ferro, cumaru da Folha Grande, cumaru true, cumari and internationally it is known as Tonka [4,5,6]. The species attracts great interest due to the uses attributed to it in popular medicine. The drug extracted from the seeds has proven therapeutic action, due to the presence of coumarin, an active ingredient generally associated with other drugs, used in the treatment of disorders of vascular and lymphatic functions, also exerting anti-inflammatory and anti-edematous action. The fruit almonds, aromatic due to the presence of coumarin, a phytochemical with bronchodilating, anti-inflammatory and antispasmodic action, give rise to an essential oil called coumarin, used in perfumeries. In the bark, there is a medicinal property frequently used as an antispasmodic, tonic and effective moderator of cardiac movements and breathing [7,8,6].

Medicinal chemistry plays a central role in understanding the molecular bases of drug action, involving the discovery, planning, identification and interpretation of the molecular mechanism of action of biologically active compounds. [9,10]. In the search for new drugs, the analysis of prototype candidates involves the consideration of pharmacodynamic and pharmacokinetic factors, as well as useful pharmacotherapeutic properties [11].

Computational tools, such as molecular docking, play a fundamental role in predicting the best molecular docking orientation between compounds and target proteins [12]. This function allows elucidating the behavior of the compound in the active site of a pathogen's key protein, as well as visualizing the molecular interactions generated by the compound and the protein [13]. This virtual approach makes it possible to perform virtual drug screening, characterize molecular structures and identify compounds with inhibitory potential.

Therefore, aiming to identify potential molecules against sars-cov-2, we conducted a computational molecular docking study to identify compounds from *D. odorata* that could act as inhibitors of the proteins of the new coronavirus. Using these organic compounds in the molecular affinity process, we sought to evaluate their inhibitory activity against essential targets of sars-cov2, crucial for the processes of viral entry and replication in cells. Thus, this study aims to investigate the antiviral potential of organic compounds from *D. odorata* in relation to sars-cov-2 targets, employing molecular coupling techniques and analyzing absorption, distribution, metabolism, excretion and toxicity properties of the compounds.

2. MATERIAL AND METHODS

2.1 Selection of Ligands

D. odorata were selected from national and international scientific databases, such as the National Center for Biotechnology information (PubMed), Scientific Electronic Library Online (Scielo), Elsevier group (Scopus) and Google Scholar . The structures of the compounds were acquired from the database (https://pubchem.ncbi.nlm.nih.gov/ accessed on September 5, 2021).

2.1 Molecular Docking

The three-dimensional structures of the three coronavirus targets were acquired from the PDB protein database (http://www.rcsb.org/, accessed on October 8, 2021) [14], with the respective codes: Spike protein (PDB ID: 6VXX), angiotensin-converting enzyme ACE2 (PDB ID: 1R42), main protein M^{pro} (PDB ID: 6LU7), while the target Receptor5 (RBD – Spike/ACE2 interaction site) was designed by Barros et al., (2020) [15].

For the molecular affinity analysis, they were prepared by removing all water molecules and other groups, such as ions, using Chimera software. 13.1 [16]. Afterwards, polar hydrogen atoms were added, the Gasteiger partial charges were calculated and the non-polar hydrogens were merged in both parts, using the Autodock Tools (ADT) program version 1.5.6. Subsequently, docking was carried out using the program AutoDock Vina [17]. With the LIGPLOT program, two-dimensional schematic representations of protein-ligand complexes were generated from the standard PDB file input. Illustrations of the points of hydrogen bond and hydrophobic interactions of the compounds with the amino acids of the viral proteins were obtained [18]. The analyzes were concentrated on the lowest energy complexes of the docking conformation, with the lowest conformation chosen for a more detailed analysis [12].

2.1 ADME-TOX Predicton

The prediction of pharmaceutical parameters was carried out using the pkCSM – pharmacokinetics software (https://biosig.lab.uq.edu.au/pkcsm/ accessed on February 4, 2022), a freely available tool [19]. The pharmacokinetic profile (ADME) and toxicity of the molecules were analyzed, namely: Benzeneacetic acid, Butein, Butin, D galactoside, Dipteryxic acid, (-)-Fisetinidol, Isoliquiritigenin, (-)-Lariciresinol, Luteolin, 5-Methoxyxanthocercin A, Sulfuretin, Taraxasterol, Vouacapenic acid, 6,4´-Dihydroxy-3´-methoxyaurone .

The parameters considered include absorption (water solubility, Caco-2 permeability, human intestinal absorption, skin permeability, P-glycoprotein I and II inhibitor), distribution (steady state volume of distribution (VDss) and permeability of the blood-brain barrier), metabolism (CYP2D6 and CYP3A4 substrate, CYP1A2, CYP2C19, CYP2C9, CYP2D6 and CYP3A4 inhibitor), excretion (OCTC renal substrate) and toxicity (AMES toxicity, maximum tolerated dose, hERG I and II inhibitor, acute oral toxicity in rats (LD50), chronic oral toxicity in rats (LOAEL), hepatotoxicity and skin sensitization) [12].

3. RESULTS AND DISCUSSION

In this in silico study, compounds originating from the chemical constitution of the species *D. odorata* were subjected to the molecular docking process, aiming to evaluate the molecular affinity with the main targets of the SARS-COV-2 virus. Furthermore, the pharmacokinetic properties related to the absorption, distribution, metabolism, excretion and toxicity of these compounds were analyzed.

A total of 672 molecular interactions were carried out, using 168 organic molecules from *D. odorata* , which were tested with four coronavirus targets: the Spike protein , the main protein (M^{pro}), the Angiotensin Converting Enzyme (ACE2), and receiver 5 (Table 1). Using computational methods, the inhibitory action of cumaru compounds was evaluated in relation to crucial proteins in the process of viral entry and infection in host cells, aiming to investigate their inhibitory potential against COVID-19.

Table 1: Results of the 672 dockings carried out with the interaction of 61 ligands with the 4 receptors (Spike, M^{pro}, ACE2 and RBD) of SARS-COV-2.

Ligands	ACE2	M^{pro}	RBD	Spike	Reference

	protein	Protein		Protein	
(±)-Balanophonin	-6.8	-7.4	-6.5	-7.7	Funasaki et al., 2016 [20]
Benzeneacetic acid	-7.6	-7.2	-6.5	-8.4	Oliveros-Bastidas et al., 2013 [21]
Benzenebutanoic acid	-4.8	-4.7	-5.5	-5.9	
Butein	-6.9	-7.3	-7.2	-8.3	Da Cunha et al., 2016 [22]
Butin	-7.2	-7.5	-6.9	-8.7	Funasaki et al., 2016 [20]
Coumarin	-5.5	-5.1	-6.5	-6.2	
7,3´-Dihydroxy-8,4´-dimethoxyisoflavone	-6.6	-7.1	-7.0	-7.6	
Dipteryxic acid	-7.8	-7.6	-7.8	-8.8	
D-galactoside	-8.1	-8.1	-7.9	-8.1	Oliveros-Bastidas et al., 2013 [21]
Eriodictyol	-7.1	-7.3	-6.9	-7.3	Funasaki et al., 2016 [20]
Spatulenol	-5.7	-5.7	-6.1	-7.8	Sousa, 2017 [23]
(-)-Fisetinidol	-7.0	-7.3	-6.8	-8.2	Garcia, 2013 [24]
Heptadecanoic acid	-4.0	-4.3	-4.6	-5.3	Oliveros-Bastidas et al., 2013 [21]
Hexadecanoic acid	-3.6	-4.2	-4.7	-4.8	
Hexadecenoic acid	-3.9	-4.3	-5.3	-4.6	
7 hydroxychromone	-5.2	-5.4	-5.7	-6.3	Funasaki et al., 2016 [20]
Isoliquiritigenin	-6.4	-6.9	-6.6	-8.0	
(-)-Lariciresinol	-7.0	-6.9	-6.5	-8.6	
Luteolin	-7.1	-7.5	-7.2	-9.0	Da Cunha et al., 2016 [22]
Mannose	-4.9	-5.2	-5.3	-6.4	Oliveros-Bastidas et al., 2013 [21]
6,4´-Dihydroxy-3´-methoxyaurone	-6.7	-7.8	-6.5	-8.9	Funasaki et al., 2016 [20]
5-Methoxyxanthocercin A	-7.2	-7.0	-7.0	-8.2	
Myo-Inositol	-5.2	-5.4	-5.2	-6.2	Oliveros-Bastidas et al., 2013 [21]
Octadecenoic acid	-4.3	-4.4	-4.8	-5.5	
9-Octadecenoic acid	-4.8	-4.7	-3.9	-4.5	
oleic acid	-4.2	-4.4	-5.3	-5.3	
Propanedioic acid	-3.8	-4.4	-4.2	-4.2	
Ribitol	-4.2	-4.7	-5.1	-5.0	
Sulfuretin	-7.0	-7.7	-6.6	-8.7	Funasaki et al., 2016 [20]
Taraxasterol	-8.7	-7.3	-7.9	-9.3	Sousa, 2017 [23]
Umbelliferone	-5.4	-5.6	-6.0	-6.4	Funasaki et al., 2016 [20]
Vouacapenic acid	-7.0	-7.2	-7.4	-9.9	
Acids					
2 Ethylcaproic acid	- 4.0	- 3.9	- 4.4	- 4.7	Bajer et al., 2018 [25]
2 Methylbutyric acid	- 3.7	- 3.9	- 4.1	- 4.2	
Acetic acid	- 3.1	- 3.0	- 3.1	- 3.1	
Benzoic acid	- 4.6	- 4.5	- 5.3	- 5.6	
Butanoic acid	- 3.5	- 3.5	- 3.7	- 3.9	
Capric acid	- 3.8	- 4.0	- 4.9	- 4.5	

Capronic acid	-3.7	-3.8	-4.3	-4.4	
Caprylic acd	-4.0	-4.0	-4.7	-4.7	
Heptanoic acid	-3.9	-3.6	-4.4	-4.6	
Isobutyric acid	-3.5	-3.6	-4.1	-4.1	
Isovaleric acid	-3.5	-3.8	-4.2	-4.1	
Lauric acid	-4.2	-4.0	-4.8	-5.0	
Linoleic acid	-4.6	-3.7	-5.1	-5.7	
Myristic acid	-4.2	-4.2	-4.7	-4.8	
Palmitic acid	-4.1	-4.1	-5.0	-4.7	
Pelargonic acid	-3.9	-4.1	-4.3	-5.1	
propanoic acid	-3.3	-3.3	-3.6	-3.5	
Alcohols					
2-Methyl-1-butanol	-3.5	-3.4	-3.6	-3.7	Bajer et al., 2018 [25]
2-Pentanol	-3.2	-3.3	-3.5	-3.8	
Phenylethyl Alcohol	-4.4	-3.9	-4.7	-5.4	
3-Methyl-2-buten-1-ol	-3.5	-3.8	-3.5	-4.0	
3-Methyl-3-buten-1-ol	-3.2	-3.7	-3.7	-3.8	
3-Methyl-3-pentanol	-3.4	-3.8	-3.6	-4.3	
4-Heptanol	-3.4	-3.5	-4.6	-4.3	
Benzyl alcohol	-4.1	-4.0	-4.6	-5.1	
Dodecanol	-3.8	-3.9	-4.4	-4.4	
2-Ethyl-1-hexanol	-3.6	-3.4	-4.4	-4.6	
1-Hexadecanol	-4.0	-3.9	-4.4	-4.8	
Hexyl alcohol	-3.2	-3.0	-3.9	-4.1	
Isoamyl alcohol	-3.1	-3.5	-3.6	-3.8	
1-Octanol	-3.5	-3.3	-4.2	-4.4	
1-Pentanol	-3.2	-3.3	-3.5	-3.7	
Tetradecanol	-4.1	-3.1	-4.7	-4.5	
Tridecanol	-3.7	-4.0	-4.9	-4.1	
Aldehydes and ketones					
(E,E)-2,4-Decanedienal	-4.1	-4.1	-4.9	-4.6	Bajer et al., 2018 [25]
2,5-Hexanedione	-3.8	-3.8	-4.1	-4.4	
(E)-2-Decennial	-3.9	-3.4	-4.6	-4.4	
2-Heptanone	-3.5	-3.5	-4.3	-3.9	
2-Nonanone	-3.3	-3.7	-4.4	-4.3	
(E)-2-Nonenal	-3.4	-3.5	-4.7	-4.3	
2-Octanone	-3.5	-3.7	-4.9	-4.2	
2-Phenylcrotonaldehyde	-4.8	-4.3	-5.5	-5.5	
(E)-2-Undecenal	-3.7	-3.5	-4.3	-4.3	
3-Methyl-1-cyclopentanone	-3.7	-3.9	-4.6	-4.5	
4-Heptanone	-3.4	-3.5	-3.8	-4.1	
4-Methylacetophenone	-4.7	-4.4	-5.4	-5.4	

Acetophenone	-4.7	-4.4	-4.9	-5.4	
Acetoin	-3.3	-4.0	-3.9	-4.0	
Benzaldehyde	-4.0	-4.2	-5.0	-4.9	
Benzophenone	-5.8	-5.9	-6.5	-6.7	
Capraldehyde	-3.7	-3.5	-4.6	-4.1	
Caproaldehyde	-3.3	-3.0	-3.8	-3.8	
(E)-Cinnamaldehyde	-4.6	-4.1	-5.2	-5.0	
Crotonaldehyde	-3.2	-3.1	-3.5	-3.3	
Phenylacetaldehyde	-4.4	-4.0	-4.9	-5.0	
Furfural	-3.6	-4.1	-4.2	-4.1	
Heptanal	-3.3	-2.9	-4.1	-3.9	
Hydroxyacetone	-3.4	-3.5	-3.3	-3.6	
Isobutanal	-3.1	-3.0	-3.3	-3.2	
Isovaleraldehyde	-3.1	-3.4	-3.8	-3.6	
Lauraldehyde	-3.6	-3.5	-4.8	-4.5	
Methyl octyl ketone	-3.9	-3.8	-4.6	-4.5	
Myristaldehyde	-3.7	-3.6	-4.3	-4.3	
o-Hydroxyacetophenone	-4.7	-4.8	-4.8	-5.4	
Octanal	-3.4	-3.2	-4.5	-4.2	
p-Anisaldehyde	-4.3	-4.1	-5.1	-5.4	
Palmitaldehyde	-3.8	-3.8	-5.4	-4.1	
Pelargonaldehyde	-3.8	-3.3	-4.1	-4.6	
Salicylaldehyde	-4.2	-4.5	-5.2	-5.1	
Aromatic hydrocarbons					
1,3-Diphenylpropane	-5.9	-5.7	-6.6	-6.2	Bajer et al., 2018 [25]
2-Methylnaphthalene	-5.7	-5.2	-6.4	-6.4	
Anthracene	-6.5	-5.8	-7.4	-7.1	
p-Xylene	-4.4	-4.0	-5.2	-5.0	
Phenylbenzene	-5.3	-5.4	-6.1	-6.1	
Toluene	-4.0	-3.9	-4.9	-4.4	
Vinylbenzene	-4.3	-3.8	-5.3	-4.9	
Esthers					
2-Ethylhexyl benzoate	-5.2	-5.1	-6.0	-5.7	Bajer et al., 2018 [25]
2-Ethylhexyl salicylate	-5.7	-5.5	-5.1	-6.1	
2-Methylbutyl acetate	-3.7	-3.9	-4.7	-4.6	
Benzyl benzoate	-6.3	-6.1	-6.6	-6.8	
Benzyl formate	-4.4	-4.3	-5.5	-4.8	
Butyl acetate	-3.7	-3.6	-3.8	-4.3	
Dibutyl phthalate	-5.4	-5.3	-5.1	-5.9	
Diethyl phthalate	-4.9	-5.1	-5.1	-6.0	
Diisobutyl phthalate	-5.8	-5.5	-5.4	-6.5	

Ethyl 2-methylbutyrate	-3.8	-3.8	-4.5	-4.5	
Ethyl benzoate	-4.5	-4.5	-5.3	-5.5	
Ethyl caproate	-3.7	-3.8	-4.7	-4.6	
Hexyl acetate	-3.8	-3.4	-4.1	-4.4	
Isoamyl acetate	-3.9	-3.7	-4.2	-4.6	
Isopropyl myristate	-3.9	-3.9	-5.4	-4.7	
Methyl isovalerate	-3.6	-3.6	-4.3	-4.2	
Methyl linoleate	-4.5	-4.3	-4.2	-5.8	
Methyl myristate	-4.2	-3.9	-5.3	-4.7	
Methyl palmitate	-4.4	-3.8	-4.6	-4.7	
Phenethyl acetate	-4.6	-4.6	-5.4	-5.2	
Aliphatic hydrocarbons					
2-Methylhexadecane	-4.0	-4.0	-5.3	-4.6	Bajer et al., 2018 [25]
3-Methylheptadecane	-4.4	-3.7	-5.3	-4.9	
Decylcyclohexane	-4.8	-4.0	-6.2	-5.2	
Dodecane	-3.7	-3.8	-5.0	-3.9	
Heptadecane	-3.7	-3.8	-5.4	-4.9	
n-Hexadecane	-4.1	-3.8	-4.8	-4.5	
Octadecane	-4.5	-3.6	-5.5	-4.5	
Pentadecane	-3.9	-3.9	-4.3	-4.3	
Phytane	-4.3	-4.2	-6.5	-4.8	
Pristane	-4.4	-4.5	-4.2	-5.7	
Squalene	-5.4	-5.9	-6.7	-6.0	
Tetradecane	-3.7	-4.1	-5.3	-4.4	
Tridecane	-3.7	-4.0	-5.1	-4.3	
Lactones					
3,4-Dihydrocoumarin	-5.3	-5.0	-6.2	-6.3	Bajer et al., 2018 [25]
Monoterpenes, monoterpenoids					
3-Carene	-4.8	-4.2	-5.4	-5.5	Bajer et al., 2018 [25]
4-Terpineol	-4.8	-4.6	-5.1	-5.7	
Carvone	-4.9	-4.7	-5.0	-5.8	
Limonene	-4.9	-4.4	-5.5	-5.1	
Linalool	-4.3	-4.3	-5.5	-5.1	
Menthol	-4.4	-4.7	-5.0	-5.3	
p-Cymene	-5.1	-4.6	-5.9	-5.3	
p-Cymenene	-5.1	-4.5	-5.9	-5.6	
Sabinene	-4.7	-4.3	-5.5	-5.0	
(Z)-Sabinene hydrate	-4.4	-4.7	-5.2	-5.6	
Terpinolene	-5.2	-4.9	-5.0	-5.5	
Others					
1,3,5,7-Cyclooctatetraene	-4.2	-4.0	-4.5	-4.6	Bajer et al., 2018 [25]
2,6-Dimethylpyrazine	-3.8	-3.8	-4.6	-5.0	
6-Methyl-5-hepten-2-one	-3.9	-3.6	-4.9	-4.6	

Benzothiazole	-4.4	-4.1	-5.0	-4.9	
Benzyl nitrile	-4.7	-4.3	-5.7	-4.9	
Coumarone	-4.6	-4.4	-5.4	-5.2	
Dibenzofuran	-5.9	-5.6	-6.4	-6.9	
Diphenylamine	-5.5	-5.6	-6.5	-5.9	
Enanthamide	-3.9	-3.5	-4.5	-4.5	
Eugenol	-5.1	-4.9	-5.8	-5.3	
o-Nitrophenol	-4.7	-4.8	-4.7	-5.4	
p-Vinylguaiacol	-5.0	-4.9	-5.1	-5.3	
Pyranone	-3.7	-3.9	-4.2	-4.3	
Pyrrole-2-carboxaldehyde	-4.0	-3.9	-4.2	-4.3	
Sesquiterpenes, sesquiterpenoids					
Caryophyllene oxide	-5.7	-5.3	-6.6	-7.6	Bajer et al., 2018 [25]

The results of the 672 molecular interactions carried out showed an energy variation between -10 kcal.mol^{-1} and -2.8 kcal.mol^{-1} . The F group stood out, presenting the most satisfactory complex interactions, with binding energies of -9.9 kcal.mol^{-1} to -8.0 kcal.mol^{-1} (Figure 1). Interactions that reached binding energy values lower than -7.9 kcal.mol^{-1} were considered most significant , totaling 17 molecular interactions (Table 2).

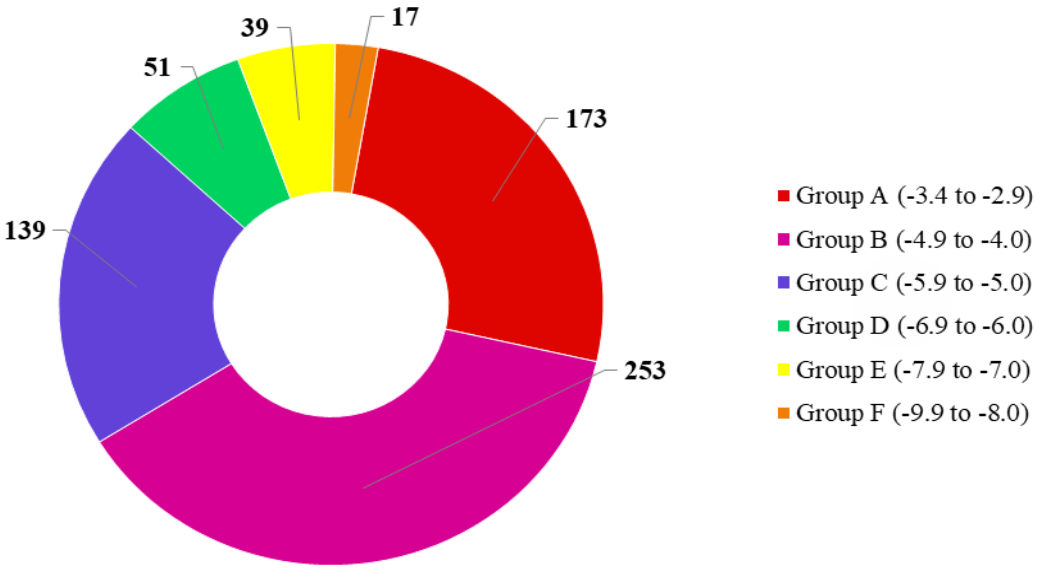

Figure 1: Total number of results, given in terms of binding energy (kcal.mol^{-1}), ordered by categories.

Table 2: Molecular affinity parameters of the chemical constituents (ligands) of the species *D. odorata* with the ACE2, Spike, and M^{pro} proteins of the new coronavirus (COVID-19) with binding energy results lower than -7.9 kcal.mol^{-1} .

Compound	ΔG $_{bind}$ ^{to} (kcal.mol^{-1})	Amino acids that interact through hydrogen	Amino acids that perform hydrophobic interaction

		bonds	
Vouacapenic acid /Spike	-9.9	Gly744, Tyr741	Ile587, Thr549, Pro589, Arg1000, Ile742, Leu966, Leu977, Phe855, Asn856, Thr572, Phe541
Taraxasterol /Spike	-9.3		Arg983, Ile973, Leu517, Thr430, Phe515, Glu516, Phe464, Asp198, Ser514, Leu518
Luteolin /Spike	-9.0	Met740, Phe855, Thr573, Arg1000, Tyr741	Asn856, Gly548, Asn978, Thr547, Leu546, Val976, Thr572, Leu966, Gly744
6,4´-Dihydroxy-3´-methoxyaurone /Spike	-8.9	Thr549, Thr573, Arg1000, Gly744	Phe541, ASn978, Thr572, Leu966, Leu977, Ile587, Pro589, Val976
Dipteryxic acid /Spike	-8.8	Thr573, Tyr741, Arg1000	Phe541, Asn978, Thr572, Val976, Leu977, Gly744, Leu966, Pro589, Asn856, Thr549, Ile587
Butin /Spike	-8.7	Arg1000, Leu977, Thr573, Met740	Tyr741, Gly744, Val976, Leu546, Asn978, Thr547, Thr572, Asn856
Sulfuretin /Spike	-8.7	Thr573, Gly744, Arg1000	Phe541, Ile587, Pro589, Thr549, Leu977, Cys743, Leu966, Ile742, Thr572
Taraxasterol /ACE2	-8.7	Asp382, Tyr385, His401	Asn51, Ser47, Ala348, Trp349
(-)-Lariciresinol /Spike	-8.6	Arg1000, Asn978, Ile587, Thr572, Gly744, Leu966	Tyr741, Thr573, Pro589, Asn856, Phe855, Val976, Ser975
Benzeneacetic acid /Spike	-8.4	Leu977, Arg1000	Asn856, Phe855, Thr572, Ser975,

			Val976, Thr573, Thr547, Pro589, Asp568
Butein /Spike	-8.3	Thr573, Gly744, Asn856, Met740, Leu977, Arg1000.	Leu546, Val976, Asn978, Thr572, Tyr741, Leu966, Thr547.
(-)-Fisetinidol /Spike	-8.2	Gly744, Asn978, Arg1000, Ile742, Tyr741, Met740	Ile587, Thr549, Thr573, Leu977, Thr572, Pro589
5-Methoxyxanthocercin A /Spike	-8.2	Gly757, Leu754, Ser975, Ser967, His519, Ser968	Asn969, Asp571, Val42, Leu518, Ala520, Asp40, Lys41, Ser50, His49, Gla755
D galactoside /Spike	-8.1	Arg44, Asp40, His49, Ser50, Ser967, Ser968, Asp571	Thr51, Ile569, Gln755, Leu754, Asn969, Gly757,
D galactoside /ACE2	-8.1	Asp382, Tyr385, Asn394, His401, Asn397	Phe400, Gly395, Glu398, Arg514, Glu402, His378
D galactoside /M ^{pro}	-8.1	Asn142, His163, Cys145, Thr26	Leu141, Glu166, Phe140, Leu27, Gly143, His41, His164, Met49, Asp187, Arg188, Met165, Gln189
Isoliquiritigenin /Spike	-8.0	Met740, Thr573, Leu977, Arg1000	ASn856, Tyr741, Gly744, Thr572, Thr547, leu546, Asn978, Leu966, Val976

D. odorata molecules that showed the most promising results in interactions with SARS-COV-2 targets are represented in two-dimensional (2D) structures in figure 2. The Spike protein was the target with the highest number of significant interactions in this study, totaling 14. As for the ACE2 protein, two interactions were obtained. Furthermore, a satisfactory result of binding energy was observed in the interaction with the M^{pro} protein, as illustrated in Figure 3.

Figure 2: Two-dimensional (2D) chemical structure of the molecules that presented the best energies in molecular affinity ((1) (Benzeneacetic acid); (2) (Butein); (3) (Butin); (4) (D galactoside); (5) (Dipteryxic acid); (6) ((-)-Fisetinidol) (7) (Isoliquiritigenin); (8) ((-)-Lariciresinol); (9) (Luteolin); (10) (5-Methoxyxanthocercin A);

(11) (Sulfuretin); (12) (Taraxasterol); (13) (Vouacapenic acid); (14) (6,4´-Dihydroxy-3´-methoxyaurone)).

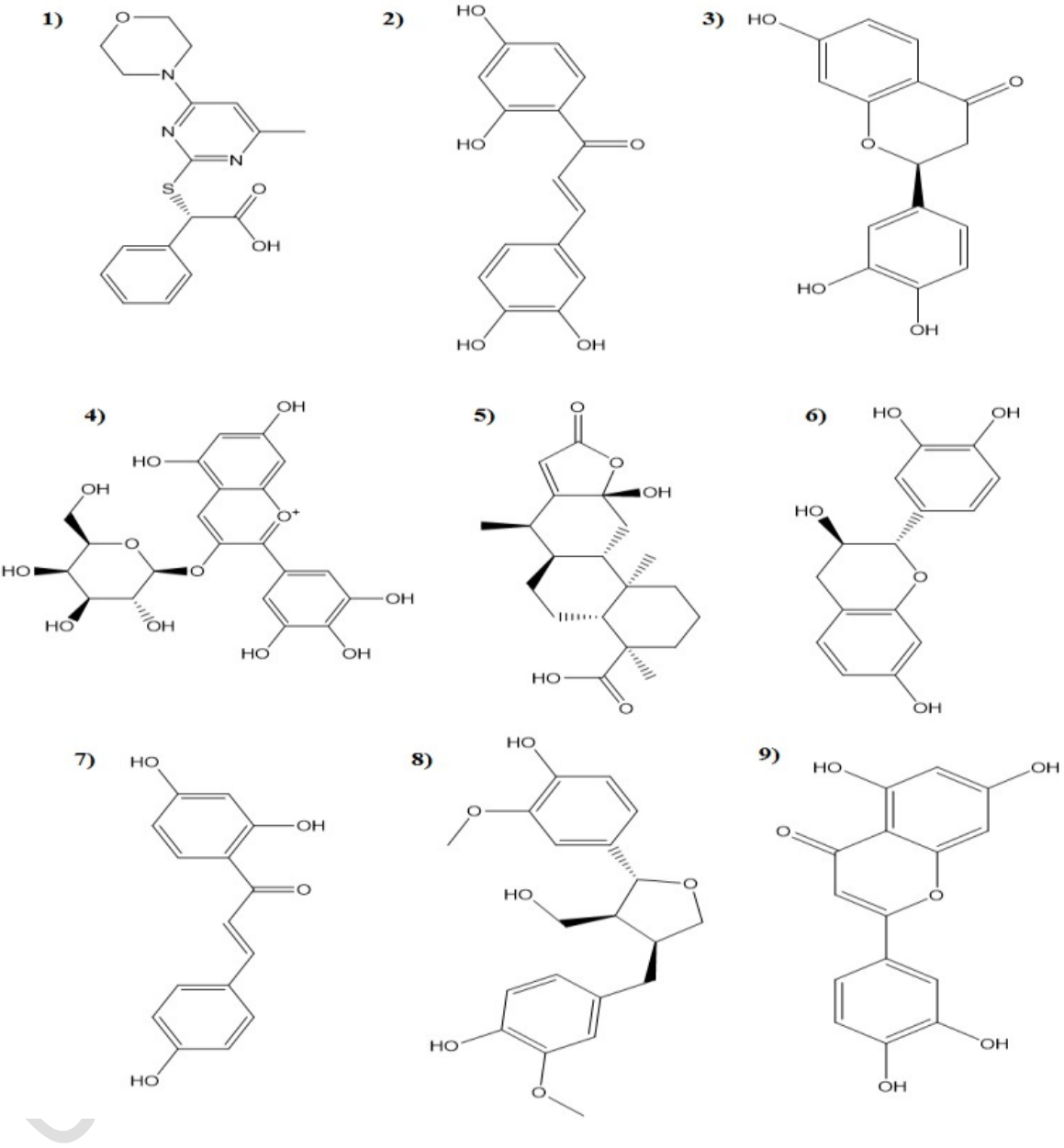

10)

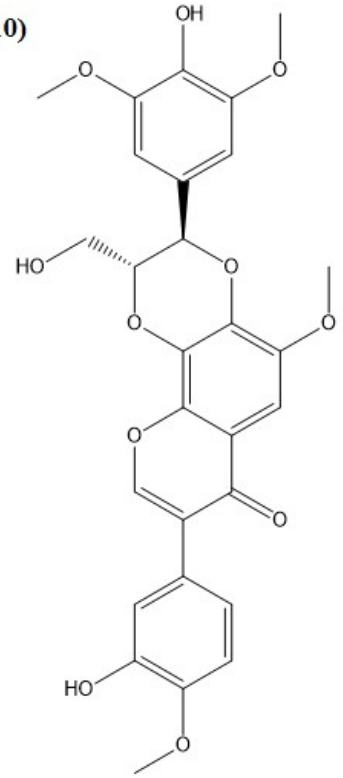

11)

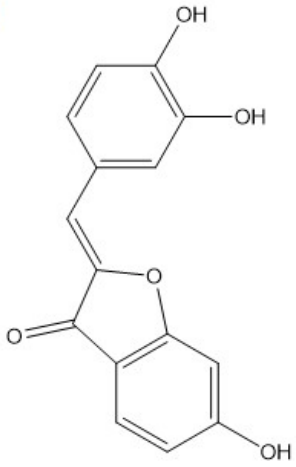

12)

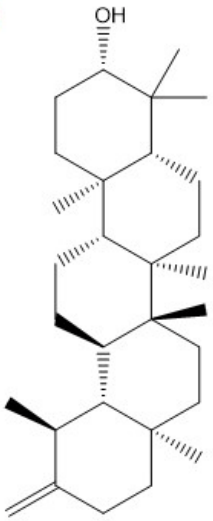

13)

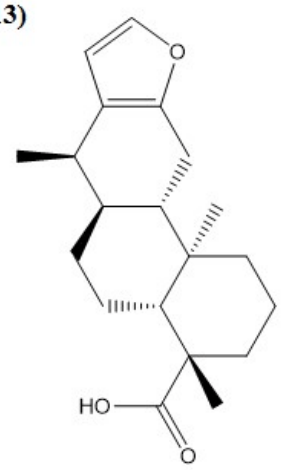

14)

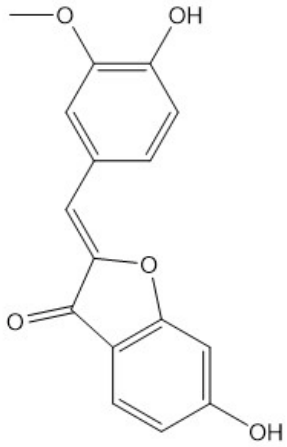

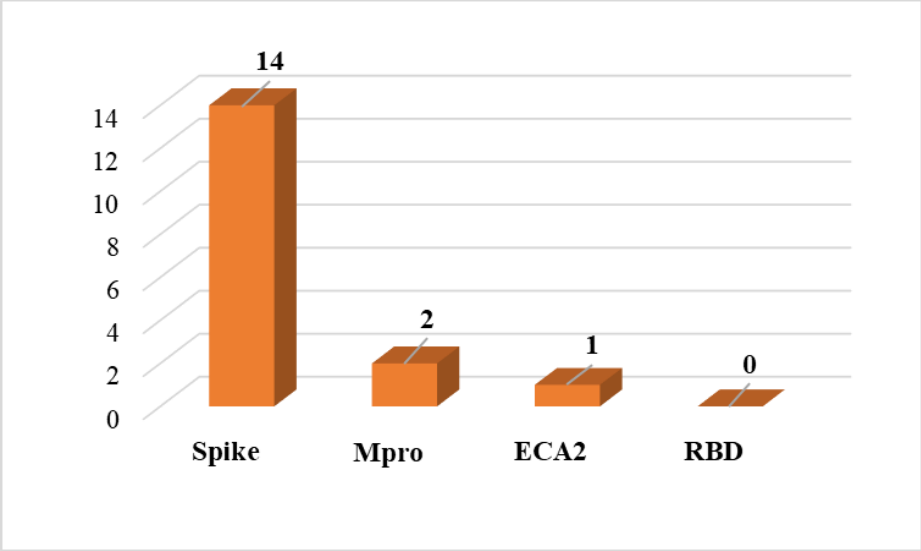

Figure 3: SARS-COV-2 proteins that demonstrated high levels of interaction with compounds from *D. odorata*.

The most satisfactory molecular affinity with binding energy equal to -9.9 kcal.mol^{-1} was identified in the interaction of vouacapenic acid with the Spike protein of the coronavirus (COVID-19), which plays a crucial role in the entry of the virus into host cells. Vouacapenic acid interacted via hydrogen bonding with the amino acids Gly744 and Tyr741, in addition to interacting via hydrophobic bonding with eleven amino acids: Ile587, Thr549, Pro589, Arg1000, Ile742, Leu966, Leu977, Phe855, Asn856, Thr572 and Phe541 (Figure 4).

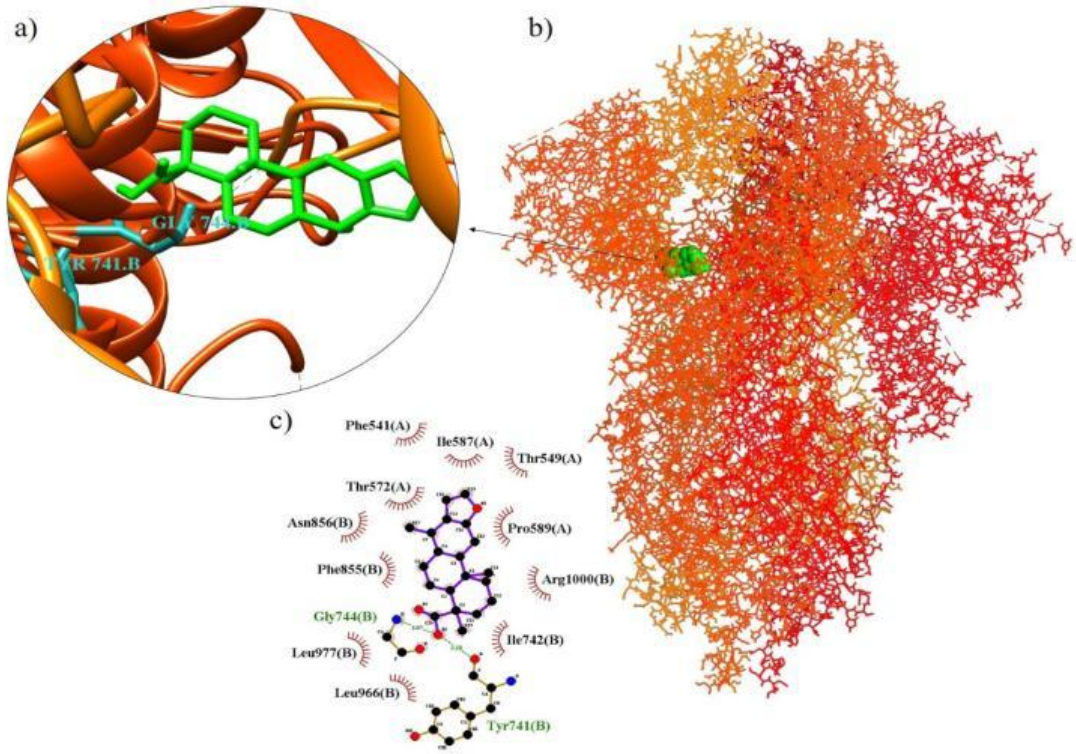

Figure 4: Three-dimensional representation of the complex formed by the vouacapenic acid ligand and the Spike protein, which obtained an interaction energy of -9.9 kcal.mol^{-1}. A) Site of interaction of the protein-ligand complex. B) 3D conformation of the vouacapenic acid compound in complex with the Spike protein. C) 2D scheme showing hydrogen (green) and hydrophobic bonds.

A total of three results showed interaction energy of the ligand with the protein (complex/ligand) lower than -8.9 kcal.mol^{-1}. In addition to vouacapenic acid , taraxasterol and luteolin stood out, with energy values of -9.3 kcal.mol^{-1} and -9.0 kcal.mol^{-1} respectively. It is important to highlight that such data were obtained through molecular coupling with the same protein, the Spike protein.

It is important to highlight that, in the molecular docking results, the presence of compounds that obtained good interactions with more than one receptor was observed, such as the ligand taraxasterol and galactoside. The compound d galactoside demonstrated satisfactory interaction results with three of the receptors analyzed. With Spike protein, ACE2 and M^{pro}, the binding energy was -8.1 kcal.mol^{-1} .

In turn, the ligand taraxasterol showed significant interactions with two targets: the Spike protein and ACE2. With the Spike protein, the interaction energy resulted in a value of -9.3 kcal.mol^{-1}, while with the ACE2 protein, an energy of -8.7 kcal.mol^{-1} was obtained (Figure 5). The ACE2 protein (angiotensin-converting enzyme) is the main receptor target of the virus in cells, due to its direct interaction with the S protein of the SARS-COV-2 virus.

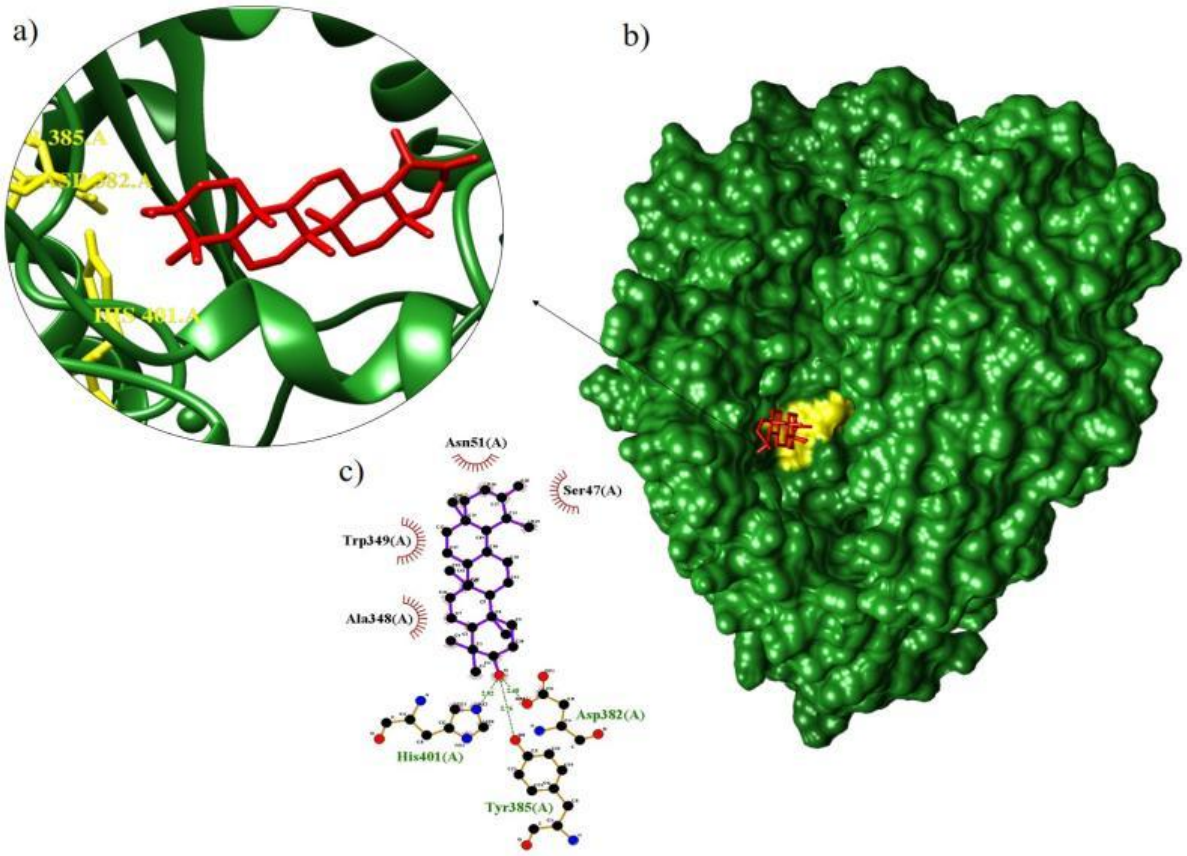

Figure 5: Three-dimensional representation of the complex formed by the taraxasterol ligand and the ACE2 protein, which obtained an interaction energy of -8.7 kcal.mol^{-1}. A) Site of interaction of the protein-ligand complex. B) 3D conformation of the taraxasterol compound in complex with the ACE2 protein. C) 2D scheme showing hydrogen (green) and hydrophobic bonds.

Regarding Receptor 5, both the d galactoside compound and taraxasterol demonstrated the best interaction energies, recording a common value of -7.9 kcal.mol^{-1} . The d-galactoside ligand showed a significant interaction with the M^{pro} protein, the target of many studies due to its crucial function in virus replication in host cells, reaching an energy value of -8.1 kcal.mol^{-1}. Additionally, hydrogen bonds were identified with the amino acids Asn142, His163, Cys145 and Thr26, in addition to hydrophobic interactions involving Leu141, Glu166, Phe140, Leu27, Gly143, His41, His164, Met49, Asp187, Arg188, Met165, Gln189 (Figure 06) .

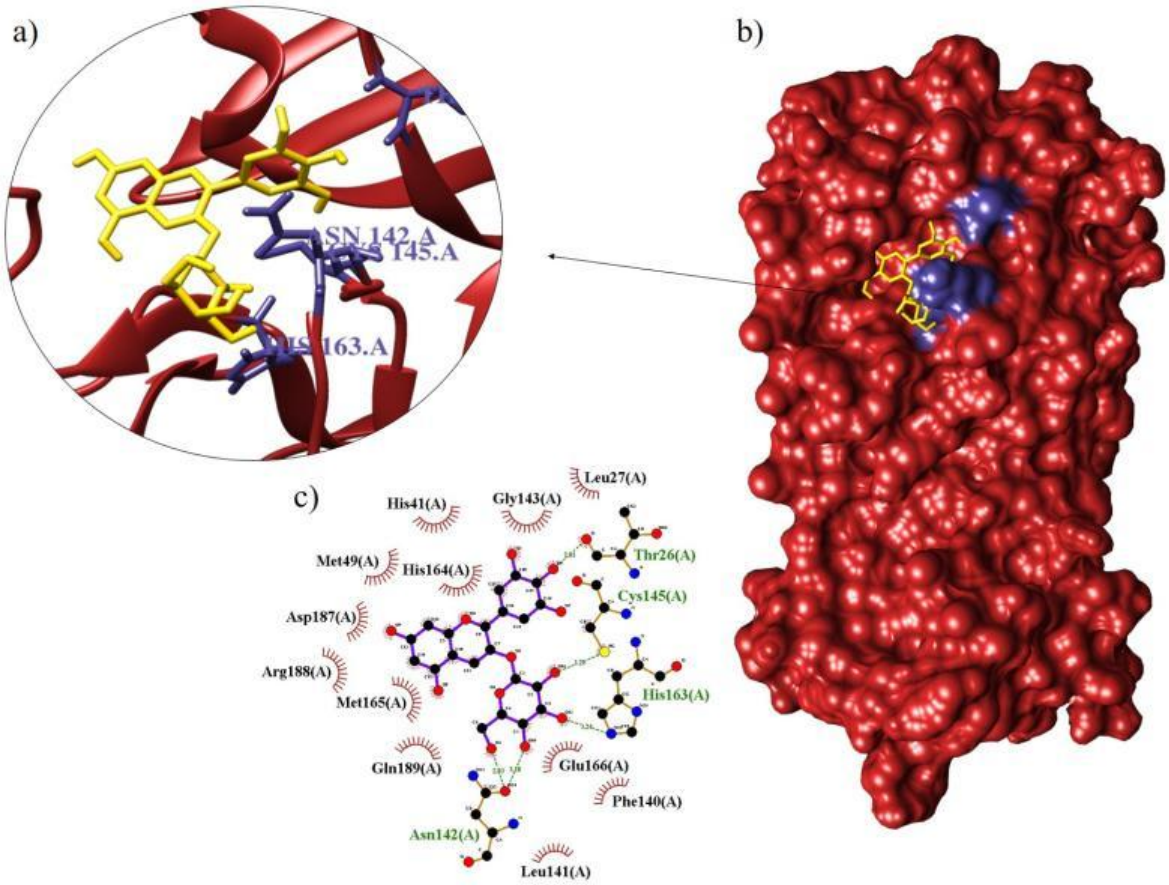

Figure 6: Three-dimensional representation of the complex formed by the d galactoside ligand and the M^{pro} protein, which obtained an interaction energy of -8.1 $kcal.mol^{-1}$. A) Site of interaction of the protein-ligand complex. B) 3D conformation of the d galactoside compound in complex with the M^{pro} protein. C) 2D scheme showing hydrogen (green) and hydrophobic bonds.

In silico molecular docking analysis revealed that certain molecules present in the plant demonstrated excellent molecular affinity with the virus targets. Among them, bioactive molecules stand out, such as taraxasterol, luteolin and isoliquiritigenin, which have received extensive research into their pharmacological properties.

The triterpenoid taraxasterol is a bioactive compound widely recognized for its presence in several medicinal plants, presenting pharmacological properties, such as anti-inflammatory, antioxidant, anticarcinogenic activities [26], and chemopreventive action [27]. The compound luteolin, a flavonoid found in several species of plants used in traditional medicine, exerts activities as an antioxidant, anti-allergic [28], anti-inflammatory [29], anticarcinogenic agent [30,31] and others. Isoliquiritigenin, a compound with anticancer, anti-inflammatory, antimicrobial and hepatoprotective [32], antitumor [33] and antioxidant [34] properties.

Phytochemicals such as taraxasterol and luteolin, present in Taraxacum officinale, were studied in silico and in vitro, demonstrating their therapeutic potential against the NS5B polymerase of the hepatitis C virus. The results indicated excellent scores in the molecular docking process, with in vitro evaluation revealing the ability of T. officinale leaf extract to

block viral replication and expression of the NS5B gene, without presenting toxic effects on normal fibroblast cells in the body [35].

Experimentally, luteolin and quercetin were evaluated in relation to the RdRp of SARS-CoV-2, an important target of the virus responsible for the COVID-19 pandemic, as conducted by Manufò et al., (2022) [36]. The results obtained, both experimental and computational, add information to previous computational investigations that proposed these two natural compounds as potential agents against COVID-19.

The results obtained in studies conducted by Souza et al., 2023 [37], Souza et al., 2023 [38] and Alves et al., 2023 [39], significantly corroborate the molecular affinity evidenced between the luteolin compound and the Spike protein.

In Brazil, the National Health Surveillance Agency (Anvisa) granted approval for the emergency use of six medicines intended for the treatment of COVID-19, starting in June 2021 [40]. Among these medications, Remdesivir, Paxlovid (nirmatrelvir + ritonavir), Molnupiravir and Baricitinib stand out, and are also recommended by the international Solidarity initiative, led by the World Health Organization (WHO) [41]. The results of the binding energy of these drugs with the SARS-COV-2 receptors are described in Table 3, demonstrating that none of the drugs presented results lower than -8.0 kcal.mol^{-1}.

Table 3: Molecular affinity parameters of the drugs Baricitinib, Molnupiravir, Paxlovid and Remdesivir with the ACE2 , M ^{pro} , ACE2 /S Complex and Spike proteins of the new coronavirus (COVID-19).

DRUG	CID	ACE2	M ^{PRO}	RBD	Spike
Baricitinib	44205240	-6.8	-7.9	-7.8	-8.0
Molnupiravir	145996610	-7.2	-6.7	-6.8	-7.9
Paxlovid (nirmatrelvir + ritonavir)	155903259	-7.1	-7.6	-7.0	-7.3
Remdesivir	121304016	-7.3	-7.9	-7.6	-7.5

Source: Own authorship, 2023

It is observed that the drugs Remdesivir and Paxlovid had a greater interaction with the M^{pro} protein, recording values of -7.9 kcal.mol^{-1} and -7.6 kcal.mol^{-1}, respectively. The other two drugs, Molnupiravir and Baricitinib, demonstrated lower molecular affinity with the Spike protein, presenting binding energies of -7.9 kcal.mol^{-1} and -8.0 kcal.mol^{-1} , respectively. In this study, the results of the interaction of *D. odorata* compounds with the targets revealed remarkable affinities, surpassing the results of the docking of drugs approved by Anvisa.

Drug repositioning is a strategy that aims to identify new therapeutic indications for molecules previously approved and used in other conditions, considered effective and safe in these contexts [42]. In this way, several medicines originally intended to treat other diseases were subjected to repositioning tests against Covid-19. Among them, we highlight the drugs that were successful in clinical trials, demonstrating anti-SARS-COV-2 therapeutic efficacy [43] and were authorized by the FDA for the treatment of patients with COVID-19, such as remdesivir [44], molnupiravir [45], baricitinib [46] and paxlovid [47].

The natural molecules investigated in the present study exhibited superior results in terms of molecular affinity with the crucial proteins of COVID-19. They presented complexes with lower energies, resulting in better inhibitory activity compared to the drugs used to treat SARS-COV-2. We therefore suggest carrying out more tests and clinical trials to deepen understanding of the action of these compounds. they have the potential to be considered as promising therapeutic agents for the treatment of COVID-19.

ADME-TOX PREDICTION

The prediction of profiles of ADME-TOX molecules (absorption, distribution, metabolism, excretion and toxicity) has been integrated into the drug research procedure, through the evaluation of their pharmacokinetic properties. This approach allows the anticipation of the presence of desirable and favorable physicochemical characteristics, identifying them as potential candidates in the context of developing new drugs [48]. The absorption prediction parameters of compounds that obtained satisfactory binding energies with SARS-COV-2 targets are described in Table 4.

Table 4: Absorption and distribution properties of *D. odorata compounds* with the best molecular interaction energies.

Compounds	**Absorption**						**Distribution**	
	Solubility in water (log mol/L)	**PCaco 2 (Log Papp at 10 - 6 cm/s)**	**AIH /% Intestinal absorption (human)**	**PSkin (log Kp)**	**P-glycoprotein I inhibitor**	**P-glycoprotein II inhibitor**	**VDss (human) (log L/kg)**	**BBB permeability**
Vouacapenic acid	-3,398	1,454	100	-2,732	No	No	-1.015	0.018
taraxasterol	-5,786	1,232	95,353	-2,741	Yes	Yes	-0.018	0.723
luteolin	-3,173	0.762	81,082	-2.735	No	No	0.071	-1.199
6,4´-Dihydroxy-3´-methoxyaurone	-3,324	1,156	94,306	-2.857	No	No	0.051	-0.189
Dipteryxic acid	-3,027	1,089	100	-2.735	No	No	-1.319	0.237
butin	-3.13	0.936	92,257	-2.739	No	No	0.259	-0.972
Sulfuretin	-3,146	1,005	93.03	-2.751	No	No	0.116	-0.948
(-)-Lariciresinol	-3.744	1,044	96,288	-2.778	No	No	0.199	-0.856
Benzeneacetic acid	-2,483	1,143	100	-2,732	No	No	-1.759	-0.73
butein	-3,042	0.599	79,621	-2.749	No	No	0.071	-0.976
(-)-Fisetinidol	-3,108	0.738	94,684	-2.735	No	No	0.556	-0.92
5-Methoxyxanthocercin A	-3,494	0.704	99,062	-2.735	Yes	Yes	-0.407	-1.769
D galactoside	-2.905	-0.872	31,243	-2.735	No	No	-0.222	-2,577
Isoliquiritigenin	-2,983	0.98	91,159	-2.977	No	No	-0.005	-0.703

Source: prepared by the author (2023)
Note: PCaco-2: Caco-2 cell permeability; AIH: human intestinal absorption potential; PSkin: skin permeability; IGp-P: P-glycoprotein inhibitor; VDss: volume of distribution at steady state; PBH: blood-brain barrier permeability.

The solubility of a compound in water has a profound impact on its absorption and distribution. Analysis of the data reveals that all compounds exhibit considerable solubility; however, it is notable that taraxasterol has been shown to be the least soluble among them. Compounds with low solubility tend to exhibit a poor absorption pattern.

The assessment of skin permeability plays an important role in the context of the development of skin medicines. All compounds demonstrated log Kp values greater than -2.3, thus indicating that they are all considered skin permeable [19].

Human colon adenocarcinoma (Caco-2) cells are associated with human intestinal absorption, enabling mechanistic assessment of drug permeability, including passive diffusion (paracellular and transcellular), transporter-mediated uptake, and transporter-mediated efflux [49]. high permeability in Caco-2 is indicated by values greater than 0.90 (PIRES et al., 2015). The compounds that demonstrated high permeability in Caco-2 cells were the following: vouacapenic acid (1,454 cm/s), taraxasterol (1,232 cm/s), 6,4´-Dihydroxy-3´-methoxyaurone (1,156 cm/s), Dipteryxic acid (1,089 cm/s), butyn (0,936 cm/s), sulfurethin (1,005 cm/s), (-)-Lariciresinol (1,044 cm/s) and the compound Benzeneacetic acid (1,143 cm/s). In contrast, the other compounds did not show satisfactory results in this aspect.

P-glycoprotein is a transmembrane ATPase that plays a significant role as a defense mechanism against harmful agents, promoting the pumping of toxins and xenobiotic substances out of cells [50]. P-gp inhibition may decrease the clearance of substrates administered intravenously, due to increased retention in the intestinal lumen and/or reduced intestinal secretion, resulting in greater renal reabsorption [51]. Among the compounds analyzed, two of them, specifically taraxasterol and 5-Methoxyxanthocercin A, demonstrated the ability to inhibit both P-glycoprotein I and II.

Intestinal absorption of a medication is a crucial factor in its oral bioavailability, allowing the medication to enter the bloodstream. Absorption in the small intestine is influenced by several elements, including the characteristics of the drug, intestinal physiology, active and passive transport mechanisms, as well as metabolism [52,53]. Molecules with absorption values between 70% and 100% are indicative of a good intestinal absorption capacity [54]. Almost all molecules analyzed in this study demonstrated significant potential for intestinal absorption, with values ranging from 79.6% to 100%. These molecules include vouacapenic acid, taraxasterol, 6,4'-Dihydroxy-3'-methoxyaurone, Dipteryxic acid, butin, Sulfuretin, (-)-Lariciresinol, Benzeneacetic acid, butein, (-)-Fisetinidol, 5-Methoxyxanthocercin A, D galactoside, Isoliquiritigenin. The only exception was the compound d galactoside, which did not show significant intestinal absorption, with a value of 31.2%.

The prediction of steady-state volume of distribution (VDss) is a fundamental pharmacokinetic parameter that, together with clearance, determines the half-life of a compound and, consequently, influences the dosing regimen [55]. VDss values below 0.71 L/K are considered low, while values above 2.81 L/K are considered high [19]. All compounds analyzed in this study demonstrated a low VDss, meaning they are more likely to be distributed into plasma rather than tissues.

Regarding the potential to penetrate the blood-brain barrier (BBB), a compound with a logBB predictive value > 0.3 is considered capable of easily crossing this barrier, while a logBB value > -1 indicates inadequate distribution in the brain [19,50]. The only compound that demonstrated the ability to cross the BBB was taraxasterol.

The superfamily of heme-containing enzymes known as CYP450 is responsible for mediating drug metabolism. The members of this superfamily, called CYPs, are heme proteins that catalyze oxidative reactions of various compounds, such as steroids, fatty acids and xenobiotics. CYPs have a prominent role in drug metabolism [56]. In the study in question, the compounds shown to inhibit the CYP3A4 substrate were vouacapenic acid, taraxasterol, dipteryxic acid and 5-Methoxyxanthocercin A, while no compound inhibited the CYP2D6 substrate. The molecules luteolin, sulphuretin and (-)-Fisetinidol only inhibited CYP1A2. The compound 6,4'-Dihydroxy-3'-methoxyaurone was shown to inhibit three enzymes (CYP1A2, CYP2C19 and CYP3A4), and the compounds that were shown to inhibit two proteins were butyn (CYP1A2 and CYP2C9), (-)-Lariciresinol (CYP2C19 and CYP2C9), butein (CYP1A2 and CYP3A4) and 5-Methoxyxanthocercin A (CYP2C9 and CYP3A4). It is important to highlight that only the compound isoliquiritigenin was shown to inhibit four enzymes, namely CYP1A2 , CYP2C19, CYP2C9 and CYP3A4 (Table 5).

Table 5: Metabolism and excretion properties of *M. oleifera compounds* with the best molecular interaction energies.

Compounds	**Metabolism**							**Excretion**
	CYP2D6 substrate	**CYP3A4 substrate**	**CYP1A2 inhibitor**	**CYP2C19 inhibitior**	**CYP2C9 inhibitior**	**CYP2D6 inhibitior**	**CYP 3A4 inhibitor**	**OCT2 Renal Substrate**
Vouacapenic acid	No	Yes	No	No	No	No	No	No
taraxasterol	No	Yes	No	No	No	No	No	No
luteolin	No	No	Yes	No	No	No	No	No
6,4´-Dihydroxy-3´-methoxyaurone	No	No	Yes	Yes	No	No	Yes	No
Dipteryxic acid	No	Yes	No	No	No	No	No	No
Butin	No	No	Yes	No	Yes	No	No	No
Sulfuretin	No	No	Yes	No	No	No	No	No
(-)-Lariciresinol	No	No	No	Yes	Yes	No	No	No
Benzeneaceti c acid	No	No	No	No	No	No	No	No
butein	No	No	Yes	No	No	No	Yes	No
(-)-Fisetinidol	No	No	Yes	No	No	No	No	No
5-Methoxyxanth ocercin A	No	Yes	No	No	Yes	No	Yes	No
D galactoside	No	No	No	No	No	No	No	No
Isoliquiritigeni	No	No	Yes	Yes	Yes	No	Yes	No

n

Source: prepared by the author (2023)

Organic cation transporter 2 (OCT2) is a transporter responsible for renal absorption. It plays an essential role in the renal clearance of ionized forms of drugs and endogenous compounds, extracting substances from the blood to the renal tubular cell [57]. The results of the analysis demonstrated that none of the molecules evaluated is a substrate for OCT2. This information is relevant for understanding the pharmacokinetic behavior of the compounds under study, especially in the context of renal elimination.

The Ames test is widely used to anticipate the genotoxicity of compounds, mainly with regard to mutagenicity, through the use of bacteria. Compounds that are predicted to be positive in the ames test have the ability to induce mutagenicity [58]. According to toxicity predictions from the Ames test, about 50% of compounds are considered non-mutagenic. This applies to the following compounds: Vouacapenic acid, taraxasterol, luteolin, Dipteryxic acid, (-)-Lariciresinol, Benzeneacetic acid and 5-Methoxyxanthocercin A (Table 6).

Table 6: Toxicity properties of compounds with the best molecular interaction energies.

Compounds	**Toxicity**							
	AMES toxicity	**Max tolerated dose (human)**	**hERG I inhibitor**	**hERG II inhibitor**	**TAO (rat) (LD50) (mol/kg)**	**TCO (rats) (LOAEL) (log mg/kg_bw/day)**	**Hepatotoxicity**	**Skin sensitization**
Vouacapenic acid	No	0.194	No	No	2,393	1984	Yes	No
taraxasterol	No	-0.495	No	Yes	2,576	0.843	No	No
luteolin	No	0.975	No	No	2.45	1,833	No	No
6,4´-Dihydroxy-3´-methoxyaurone	Yes	0.529	No	No	1991	1,891	No	No
Dipteryxic acid	No	-0.208	No	No	2,297	0.898	No	No
Butin	Yes	0.38	No	No	2,112	2,304	No	No
Sulfuretin	Yes	0.315	No	Yes	1,901	2022	No	No
(-)-Lariciresinol	No	0.309	No	Yes	2.07	2,148	No	No
Benzeneacetic acid	No	0.842	No	No	2,457	0.85	Yes	No
butein	Yes	0.471	No	No	1,829	2,505	No	No
(-)-Fisetinidol	Yes	0.368	No	No	1.71	2,225	No	No
5-Methoxyxant	No	0.453	No	Yes	2.48	3,206	No	No

hocercin A								
D galactoside	Yes	0.624	No	Yes	2,645	3,472	No	No
Isoliquiritigenin	Yes	0.421	No	No	1961	1,502	No	No

Source: prepared by the author (2023)
Note: TAMES: AMES toxicity; DMT: Maximum tolerated dose; TAO: Acute Oral Toxicity in Rat; TCO: Chronic oral toxicity in rats.

Acute oral toxicity in rats refers to the probable lethal dose 50 (LD50) of a given compound, which is the amount in mol/kg necessary to cause the death of 50% of the animals tested. Among the compounds evaluated, galactoside showed a high LD50, while the lowest value was observed for the compound (-)-Fisetinidol. On the other hand, chronic oral toxicity in rats involves determining the lowest observable adverse effect level (LOAEL) for a specific compound. Two compounds demonstrated high LOAEL, namely 5-Methoxyxanthocercin A and galactoside D.

The recommended maximum tolerated dose (MRTD) is an estimate of the toxic dose of compounds in the body, which aims to determine a safe initial dosage of the drug. Compounds with MRTD values less than or equal to 0.477 log(mg/kg/day) are classified as low toxicity, while higher values are considered high toxicity [50]. The compounds vouacapenic acid, taraxasterol, dipteryxic acid, butyn, sulfurethin, (-)-lariciresinol, butein, (-)-fisetinidol and 5-Methoxyxanthocercin A demonstrated low MRTD values, indicating low toxicity. On the other hand, the other compounds analyzed presented high MRTD values, suggesting greater toxicity. It is important to highlight that none of the compounds demonstrated susceptibility to cause skin sensitization, which is a relevant adverse effect for products applied to the skin.

Hepatotoxicity is a significant concern in the drug development process, being one of the main causes of failure. Substances that cause hepatotoxicity can lead to serious effects, such as drug-induced liver damage, resulting in acute liver failure [59].Only two acid compounds showed signs of causing liver dysfunction, vouacapenic acid and benzeneacetic acid.

The inhibition of potassium channels encoded by the hERG gene represents the main cause of the development of acquired long QT syndrome, consequently resulting in severe and potentially lethal ventricular arrhythmias [60]. Predictions indicate that no compound demonstrates a propensity to inhibit hERGI, while five compounds were identified as possible inhibitors of hERG II, namely: taraxasterol, sulphuretin, (-)-lariciresinol, 5-Methoxyxanthocercin A and galactoside.

4. CONCLUSION

The results of this molecular affinity study between *D. odorata* molecules and SARS-COV-2 proteins were highly promising. We identified 17 compounds with the best binding energies, which showed superior interaction affinities to drugs approved by the FDA for treating COVID-19. Molecular docking showed that vouacapenic acid, taraxasterol and luteolin demonstrated excellent affinity with the Spike protein, suggesting their potential as candidates for drugs against viral entry into cells. Furthermore, these compounds exhibited positive results in the evaluation of the ADME-TOX profile, indicating their feasibility for future studies in the development of anti-SARS-COV-2 therapeutic agents. However, to advance the innovation and development of new anti-COVID-19 compounds, it is necessary to validate these results through in vivo and in vitro studies of natural compounds from *D.*

odorata. This work offers a promising starting point for developing an effective drug against the SARS-COV-2 pathogen.

CONSENT AND ETHICAL APPROVAL

It is not applicable.

REFERENCES

1. Florindo HF, Kleiner R, Vaskovich-Koubi D, Acúrcio RC, Carreira B, Yeini E, et al. Immune-mediated approaches against COVID-19. Nat Nanotechnol. 2020;15(8):630–45.
2. Zhou P, Yang X-L, Wang X-G, Hu B, Zhang L, Zhang W, et al. A pneumonia outbreak associated with a new coronavirus of probable bat origin. Nature. 2020;579(7798):270–3.
3. Mitev V. Comparison of treatment of COVID-19 with inhaled bromhexine, higher doses of colchicine and hymecromone with WHO-recommended paxlovid, molnupiravir, remdesivir, anti-IL-6 receptor antibodies and baricitinib. Pharmacia. 2023;70(4):1177–93.
4. 4. BESSA DTO, MENDONÇA MS de, ARAÚJO MGP de. Morpho-anatomy of seeds of Dipteryx odorata (Aubl.) Will. (Fabaceae) as a contribution to the pharmacognostic study of plants from the Amazon Region. Acta Amaz. 2001;31:357.
5. 5. da Silva JAG, Pauletto D, da Silva AF, de Souza Carvalho C do S, do Nascimento HGG. Morphometry of plantings of Dipteryx odorata Aubl Willd (Cumaru) in Western Pará. Adv For Sci. 2020;7(3):1171–80.
6. 6. Nicaretta B, da Silva RC, Dias C, Crexi VT, Morais MM. Extraction of Cumaru almond oil by pressing (Dipteryx odorata). An of the Int Teaching, Research and Extension Salon. 2017;9(2).
7. 7. Portela JGA, Pauletto D. Bibliometric analysis of Brazilian scientific production on Dipteryx odorata from 2009 to 2018. Rev Ibero-Americana Ciências Ambient. 2020;11(1):19–28.
8. 8. da Silva GM, de Sousa MLR, Rocha WC, de Freitas ADG. Chemical and Antimicrobial Study of Seed and Leaf Extracts of Cumaru, Dipteryx odorata (Fabaceae). Trials and Science C Biological Agricultural and Health. 2021;25(1):34–8.
9. 9. Carvalho I, Pupo MT, Borges ÁDL, Bernardes LSC. Introduction to molecular modeling of drugs in the medicinal chemistry experimental course. Quim Nova. 2003;26:428–38.
10. 10. Guido RVC, Andricopulo AD. Molecular modeling of drugs. Rev Process Químicos. 2008;2(4):24–36.
11. 11. Barreiro EJ, Rodrigues CR, Albuquerque MG, Sant'Anna CMR de, Alencastro RB de. Molecular modeling: a tool for rational drug planning in medicinal chemistry. Quim Nova. 1997;20:300–10.

12. 12. Rocha JA, Rego NCS, Carvalho BTS, Silva FI, Sousa JA, Ramos RM, et al. Computational quantum chemistry, molecular docking, and ADMET predictions of imidazole alkaloids of Pilocarpus microphyllus with schistosomicidal properties. PLoS One. 2018;13(6):e0198476.
13. 13. Meng X-Y, Zhang H-X, Mezei M, Cui M. Molecular docking: a powerful approach for structure-based drug discovery. Curr Comput Aided Drug Des. 2011;7(2):146–57.
14. 14. Berman HM, Westbrook J, Feng Z, Gilliland G, Bhat TN, Weissig H, et al. The protein data bank. Nucleic Acids Res 2000;28(1):235–42.
15. 15. Barros, R.O.; Junior, F.L.C.C.; Pereira, W.S.; Oliveira, N.M.N.; Ramos, R.M. Interaction of Drug Candidates with Various SARS-CoV-2 Receptors: An in Silico Study to Combat COVID-19. J. Proteome Res. 2020, 19, 4567–4575.
16. 16. Pettersen, E. F.; Goddard, T.D.; Huang, C.C.; Couch, G.S.; Greenblatt, D. M.; Meng, E.C.; Ferrin, T.E. UCSF Chimera?A visualization system for exploratory research and analysis. J. Computing. Chem. 2004, 25, 1605–1612.
17. 17. Trott, O.; Olson, A.J. AutoDock Vina: Improving the speed and accuracy of docking with a new scoring function, efficient optimization, and multithreading. J. Computing. Chem. 2010, 31, 455–461.
18. 18. Wallace, A.C.; Laskowski, R.A.; Thornton, J.M. Ligplot: A program to generate schematic diagrams of protein-ligand interactions. Protein Eng 1995, 8, 127–134.
19. 19. Pires, D.E.V.; Blundell, T. L.; Ascher, D.B. pkCSM: Predicting Small-Molecule Pharmacokinetic and Toxicity Properties Using Graph-Based Signatures. J. Med. Chem. 2015, 58, 4066–4072.
20. 20. Funasaki M, Barroso H dos S, Fernandes VLA, Menezes IS. Amazon rainforest cosmetics: chemical approach for quality control. Quim Nova. 2016;39:194–209.
21. 21. Oliveros-Bastidas A de J, Demuner AJ, Barbosa LC de A. Chemical characterization by GC-MS and phytotoxic potential of non-polar and polar fractions of seeds of Dioteryx odorata (Aubl.) Willd. From Venezuelan regions. Quim Nova. 2013;36:502–6.
22. 22. Da Cunha CP, Godoy RLO, Braz FR. Isolation of flavonoids from Dipteryx odorata by high-performance liquid chromatography. Rev Virtual Química. 2016;8:43–56.
23. 23. Sousa BCM de. Dipteryx odorata (Aubl.) Willd. And Dipteryx magnifica (Ducke) Ducke (FABACEAE): phytochemical characterization regarding the presence of coumarin and antifungal and antibacterial activities. Federal University of Western Pará; 2017.
24. 24. Garcia MG. Study of the chemical constituents of wood residues of Andira Parviflora, Dipteryx odorata and Swartzia laevicarpa (Fabaceae). 2013.
25. 25. Bajer T, Surmová S, Eisner A, Ventura K, Bajerová P. Use of simultaneous distillation-extraction, supercritical fluid extraction and solid-

phase microextraction for characterization of the volatile profile of Dipteryx odorata (Aubl.) Willd. Ind Crops Prod. 2018;119:313–21.
26. 26. Jiao F, Tan Z, Yu Z, Zhou B, Meng L, Shi X. The phytochemical and pharmacological profile of taraxasterol. Front Pharmacol. 2022;13:927365.
27. 27. Ovesnaâ Z, Lkovaâ AV, Thovaâ KH. Taraxasterol and b-sitosterol: new naturally occurring compounds with chemoprotective/chemopreventive effects Minireview. Neoplasm. 2004;51(6):407.
28. 28. Seelinger G, Merfort I, Schempp CM. Anti-oxidant, anti-inflammatory and anti-allergic activities of luteolin. Planta Med 2008;74(14):1667–77.
29. 29. Aziz N, Kim M-Y, Cho JY. Anti-inflammatory effects of luteolin: A review of in vitro, in vivo, and in silico studies. J Ethnopharmacol. 2018;225:342–58.
30. 30. Imran M, Rauf A, Abu-Izneid T, Nadeem M, Shariati MA, Khan IA, et al. L uteolin, a flavonoid, as an anticancer agent: A review. Biomed Pharmacother. 2019;112:108612.
31. López-Lázaro M. Distribution and biological activities of the flavonoid luteolin. Mini Rev Med Chem. 2009;9(1):31–59.
32. Peng F, Du Q, Peng C, Wang N, Tang H, Xie X, et al. A review: the pharmacology of isoliquiritigenin. Phyther Res. 2015;29(7):969–77.
33. Yamamoto S, Aizu E, Jiang H, Nakadate T, Kiyoto I, Wang JC, et al. The potent anti-tumor-promoting agent isoliquiritigenin. Carcinogenesis. 1991;12(2):317–23.
34. Shi D, Yang J, Jiang Y, Wen L, Wang Z, Yang B. The antioxidant activity and neuroprotective mechanism of isoliquiritigenin. Free Radic Biol Med. 2020;152:207–15.
35. Rehman S, Ijaz B, Fatima N, Muhammad SA, Riazuddin S. Therapeutic potential of Taraxacum officinale against HCV NS5B polymerase: In-vitro and In silico study. Biomed Pharmacother. 2016;83:881–91.
36. Munafò F, Donati E, Brindani N, Ottonello G, Armirotti A, De Vivo M. Quercetin and luteolin are single-digit micromolar inhibitors of the SARS-CoV-2 RNA-dependent RNA polymerase. Sci Rep. 2022;12(1):10571.
37. Souza MDA, Souza HCA, Viana EKA, Alves SKS, Sousa CS, Ribeiro ASN, et al. An In silico Analysis Study of the Chemical Compounds from the Crassulaceous Plant Bryophyllum pinnatum (Lam.) Oken against the SARS-COV-2 Proteases. J Adv Med Med Res. 2023;35(23):69–91.
38. Souza HCA, Souza MDA, Sousa CS, Viana EKA, Alves SKS, Marques AO, et al. Molecular Docking and ADME-TOX Profiling of Moringa oleifera Constituents against SARS-CoV-2. Adv Respir Med. 2023;91(6):464–85.
39. Alves SKS, Sousa CS, Viana EKA, Souza HCA, Souza MDA, Ribeiro ASN, et al. Bioactive components of Myracrodruon urundeuva against SARS-CoV-2: a computational study. Drugs Drug Candidates. 2023;2(4):781–95.
40. Approved Drugs-National Health Surveillance Agency-Anvisa. Available online: https://www.gov.br/anvisa/pt-br/assuntos/ paf/coronavirus/medicamentos (accessed on 8 April 2022).
41. Ferreira, L.L.G.; Andricopulo, A.D. Medicines and treatments for COVID-19. Adv. Stud. 2020, 34, 7–27.

42. Sultana, J. et al. Challenges for Drug Repurposing in the COVID-19 Pandemic Era. Front. Pharmacol. 11, 1–13 (2020).
43. Atluri K, Aimlin I, Arora S. Current effective therapeutics in management of COVID-19. J Clin Med. 2022;11(13):3838.
44. FDA. FDA approves first treatment for COVID-19. FDA press release. 2020. Accessed May 12, 2022. https://www.fda.gov/news-events/press-announcements/fda-approves-first-treatment-covid-19
45. FDA. Coronavirus (COVID-19) Update: FDA Authorizes Additional Oral Antiviral for Treatment of COVID-19 in Certain Adults | FDA. FDA press release. 2021. Accessed May 12, 2022. https://www.fda.gov/news-events/press-announcements/coronavirus-covid-19-update-fda-authorizes-additional-oral-antiviral-treatment-covid- 19-certain
46. FDA. Coronavirus (COVID-19) update: FDA authorizes drug combination to treat COVID-19. FDA press release. 2020. Accessed May 12, 2022. https://www.fda.gov/news-events/press-announcements/coronavirus-covid-19-update-fda-authorizes-drug-combination-treatment-covid-19
47. FDA. Coronavirus (COVID-19) update: FDA authorizes first oral antiviral for treatment of COVID-19 | FDA. FDA press release. 2021. Accessed May 12, 2022. https://www.fda.gov/news-events/press-announcements/coronavirus-covid-19-update-fda-authorizes-first-oral-antiviral-treatment-covid- 19
48. Ekins S, Ring BJ, Grace J, McRobie-Belle DJ, Wrighton SA. Present and future in vitro approaches for drug metabolism. J Pharmacol Toxicol Methods. 2000;44(1):313–24.
49. Volpe DA. Drug-permeability and transporter assays in Caco-2 and MDCK cell lines. Future Med Chem. 2011;3(16):2063–77.
50. Belal A. Drug likeness, targets, molecular docking and ADMET studies for some indolizine derivatives. Die Pharm Int J Pharm Sci. 2018;73(11):635–42.
51. Varma MVS, Ashokraj Y, Dey CS, Panchagnula R. P-glycoprotein inhibitors and their screening: a perspective from bioavailability enhancement. Pharmacol Res. 2003;48(4):347–59.
52. Bohets H, Annaert P, Mannens G, Anciaux K, Verboven P, Meuldermans W, et al. Strategies for absorption screening in drug discovery and development. Curr Top Med Chem. 2001;1(5):367–83.
53. Lennernas H. Modeling gastrointestinal drug absorption requires more in vivo biopharmaceutical data: experience from in vivo dissolution and permeability studies in humans. Curr Drug Metab. 2007;8(7):645–57.
54. Zhao YH, Le J, Abraham MH, Hersey A, Eddershaw PJ, Luscombe CN, et al. Evaluation of human intestinal absorption data and subsequent derivation of a quantitative structure–activity relationship (QSAR) with the Abraham descriptors. J Pharm Sci. 2001;90(6):749–84.
55. Berellini G, Springer C, Waters NJ, Lombardo F. In silico prediction of volume of distribution in human using linear and nonlinear models on a 669 compound data set. J Med Chem. 2009;52(14):4488–95.
56. Zhong HA, Mashinson V, Woolman TA, Zha M. Understanding the molecular properties and metabolism of top prescribed drugs. Curr Top Med Chem.

2013;13(11):1290–307.
57. Chen Y, Li S, Brown C, Cheatham S, Castro RA, Leabman MK, et al. Effect of genetic variation in the organic cation transporter 2, OCT2, on the renal elimination of metformin. Pharmacogenet Genomics. 2009;19(7):497.
58. Xu C, Cheng F, Chen L, Du Z, Li W, Liu G, et al. In silico prediction of chemical Ames mutagenicity. J Chem Inf Model. 2012;52(11):2840–7.
59. Gomez-Lechon MJ, Lahoz A, Gombau L, Castell J V, Donato MT. In vitro evaluation of potential hepatotoxicity induced by drugs. Curr Pharm Des. 2010;16(17):1963–77.
60. Flores-Holguín N, Frau J, Glossman-Mitnik D. Computational Pharmacokinetics Report, ADMET Study and Conceptual DFT-Based Estimation of the Chemical Reactivity Properties of Marine Cyclopeptides. ChemistryOpen. 2021;10(11):1142–9.